

See discussions, stats, and author profiles for this publication at: <https://www.researchgate.net/publication/23298731>

# Interfacial Approach to Polyaromatic Hydrocarbon Toxicity: Phosphoglyceride and Cholesterol Monolayer Response to Phenanthrene, Anthracene, Pyrene, Chrysene, and Benzo[a]pyrene

ARTICLE *in* THE JOURNAL OF PHYSICAL CHEMISTRY B · NOVEMBER 2008

Impact Factor: 3.3 · DOI: 10.1021/jp804080h · Source: PubMed

---

CITATIONS

7

READS

35

7 AUTHORS, INCLUDING:



Tapani Viitala

University of Helsinki

70 PUBLICATIONS 930 CITATIONS

[SEE PROFILE](#)



Feidt Cyril

University of Lorraine

119 PUBLICATIONS 1,117 CITATIONS

[SEE PROFILE](#)



Catherine Corbier

University of Lorraine

49 PUBLICATIONS 1,085 CITATIONS

[SEE PROFILE](#)



Ewa Rogalska

University of Lorraine

72 PUBLICATIONS 1,354 CITATIONS

[SEE PROFILE](#)

# Interfacial Approach to Polyaromatic Hydrocarbon Toxicity: Phosphoglyceride and Cholesterol Monolayer Response to Phenanthrene, Anthracene, Pyrene, Chrysene, and Benzo[a]pyrene

Beata Korchowiec,<sup>†,‡</sup> Yohann Corvis,<sup>‡,§</sup> Tapani Viitala,<sup>||</sup> Cyril Feidt,<sup>⊥</sup> Yann Guiavarch,<sup>⊥</sup> Catherine Corbier,<sup>⊥</sup> and Ewa Rogalska<sup>\*</sup><sup>‡</sup>

Department of Physical Chemistry and Electrochemistry, Faculty of Chemistry, Jagiellonian University, ul. Romana Ingardena 3, 30-060 Krakow, Poland, Structure et Réactivité des Systèmes Moléculaires Complexes, BP 239, CNRS/Nancy Université, 54506 Vandoeuvre-lès-Nancy cedex, France, KSV Instruments Ltd., Höylämötie 7, 00380 Helsinki, Finland, and URAFPA, Nancy Université, BP 239, 54506 Vandoeuvre-lès-Nancy, France

Received: May 8, 2008; Revised Manuscript Received: August 19, 2008

Interactions of phenanthrene, anthracene, pyrene, chrysene, and benzo[a]pyrene (polyaromatic hydrocarbons) with model phospholipid membranes were probed using the Langmuir technique. The lipid monolayers were prepared using 1,2-dipalmitoyl-*sn*-glycero-3-phosphocholine, 1,2-dipalmitoyl-*sn*-glycero-3-phosphoethanolamine, 1,2-dipalmitoyl-*sn*-glycero-3-phosphoglycerol, 1,2-dipalmitoyl-*sn*-glycero-3-phosphoserine, 1,2-myristoyl-*sn*-glycero-3-phosphoethanolamine, 1,2-dilauroyl-*sn*-glycero-3-phosphocholine, and cholesterol. Surface pressure and electrical surface potential were measured on mixed phospholipid/PAH monolayers spread on a pure water subphase. The morphology of the mixed monolayers was followed with Brewster angle microscopy. Polarization-modulation infrared reflection–absorption spectroscopy spectra obtained on DPPE/benzo[a]pyrene showed that the latter interacts with the carbonyl groups of the phospholipid. On the other hand, the activity of phospholipase A2 toward DLPC used as a probe to locate benzo[a]pyrene in the monolayers indicates that the polyaromatic hydrocarbons are not accessible to the enzyme. The results obtained show that all PAHs studied affect the properties of the pure lipid, albeit in different ways. The most notable effects, namely, film fluidization and morphology changes, were observed with benzo[a]pyrene. In contrast, the complexity of mixed lipid monolayers makes the effect of PAHs difficult to detect. It can be assumed that the differences observed between PAHs in monolayers correlate with their toxicity.

## 1. Introduction

Polycyclic aromatic hydrocarbons (PAHs) include hundreds of chemicals formed during the incomplete combustion of organic material.<sup>1–3</sup> PAHs, which are found throughout the environment in air, water, and soil, have attracted considerable attention because of their resistance to microbial degradation and potential toxicity for higher organisms.<sup>4,5</sup> Indeed, several PAHs, including benz[a]anthracene, benzo[a]pyrene, benzo[b]-fluoranthene, benzo[j]fluoranthene, benzo[k]fluoranthene, chrysene, dibenz[a,h]anthracene, and indeno[1,2,3-c,d]pyrene, have caused tumors in laboratory animals.<sup>1–3,6</sup> Other effects,<sup>7</sup> which may affect reproduction, development, and immunity are not well-known.<sup>6,8,9</sup> PAHs are highly hydrophobic,<sup>10</sup> which results in their accumulation in fatty tissues with a subsequent biomagnification in the food chain.<sup>11</sup> Interestingly, a different transfer rate of PAHs with comparable hydrophobicity, such as phenanthrene, pyrene, or benzo[a]pyrene, was observed in the food chain,<sup>12–14</sup> in CACO-2 intestinal cell cultures,<sup>15</sup> and MAC-T mammalian cell cultures.<sup>16</sup>

As the cytoplasmic membrane controls the transport of molecules into the cell, elucidation of the fundamental mechanisms that determine their interactions with the membrane is of crucial theoretical and practical importance. In general, cellular permeability is proportional to molecule hydrophobicity. Indeed, the Overton rule of lipid membrane permeation<sup>17</sup> states that permeation of solutes through lipid membranes is proportional to their oil–water partitioning.<sup>18</sup> The increased permeation rate is explained by a high partition coefficient,  $K_{ow}$ , of solutes, which increases the solute gradient within the transport phase.<sup>19</sup> Not surprisingly, a good correlation is often found between the toxicity of a given organic chemical and its  $K_{ow}$  value.<sup>20</sup> Voltammetry studies showed that anthracene, phenanthrene, pyrene, benzo[a]anthracene, fluoranthene, and perylene permeate dioleoylphosphatidylcholine monolayers adsorbed on a mercury electrode, from dilute aqueous solutions. The rates of penetration decreased with the increasing solubility of PAHs in water;<sup>21,22</sup> the order of affinity for the lipid layer was benzo[a]anthracene > fluoranthene, pyrene > anthracene, phenanthrene.<sup>23</sup> It was observed recently that the permeation of PAHs into lipid membranes is facilitated by heavy metal cations. It was proposed that metal complexation may neutralize the negative charge of the bacterial surface, making it less hydrophilic and enhancing hydrophobic partition of the organic solute.<sup>24</sup>

\* Corresponding author. E-mail: rogalska@lesoc.uhp-nancy.fr.

<sup>†</sup> Jagiellonian University.

<sup>‡</sup> Structure et Réactivité des Systèmes Moléculaires Complexes, CNRS/Nancy Université.

<sup>§</sup> Present address: Laboratoire de Chimie Physique, Université Paris Descartes, Faculté de Pharmacie, 4 Avenue de l’Observatoire, 75006 Paris, France.

<sup>||</sup> KSV Instruments Ltd.

<sup>⊥</sup> URAFPA, Nancy Université.

The modification of the structure and the dynamics of the lipid membranes upon interactions with PAHs may be one more reason for the cellular toxicity, besides membrane permeability.

Some results suggest that PAHs can be involved in specific interactions with cholesterol domains of the cell membrane. The subsequent changes in membrane fluidity and architecture induced by these specific interactions may modulate the distribution and/or activity of membrane proteins, which are critical to the regulation of cellular proliferation.<sup>25</sup> The effect of pyrene, benzo[a]pyrene, and anthracene on the thermotropic behavior of model membranes prepared with dimyristoylphosphatidylcholine (DMPC) was investigated by differential scanning calorimetry (DSC). These hydrocarbons, when dispersed in the DMPC vesicles, had a different impact on the gel-to-liquid crystal phase transition. Indeed, pyrene and benzo[a]pyrene shifted transition temperature toward lower values with a concomitant decrease of the associated enthalpy changes, while anthracene did not significantly affect the thermotropic behavior of the lipid vesicles. These results were interpreted in terms of a higher fluidization of the lipid bilayer by the large PAH molecules compared to the small ones.<sup>26,27</sup> On the other hand, the results obtained using DSC and electron paramagnetic resonance spectroscopy suggest that polycyclic aromatic hydrocarbons are able to modify the internal dynamics of erythrocyte membranes; this might lead to the damage of the biological functions of the membrane.<sup>28</sup>

It has to be noted that PAHs can enter microbial cells not only by passive diffusion but also by active transport, as demonstrated in the case of phenanthrene, anthracene, fluoranthene, and pyrene.<sup>29–33</sup> However, for a selective uptake and excretion of substrates and metabolites by protein carriers embedded in the membrane an optimal fluidity, stability, and permeability of the lipid layer is required.<sup>34,35</sup> The permeability can be adjusted in living cells by different mechanisms, including the modification of the fatty acids.<sup>31,36–38</sup> A possible link between the PAH uptake and membrane fluidity was suggested recently.<sup>4</sup> It was found as well that in F258 hepatic cells the benzo[a]pyrene-induced apoptosis was dependent upon the transmembrane transporter NHE1, which may be activated by alterations in the membrane. Indeed, benzo[a]pyrene induces membrane fluidization linked to NHE1 activation, while membrane stabilization by exogenous cholesterol protects cells from benzo[a]pyrene-induced apoptosis.<sup>39</sup>

The importance of the research on membrane structure–function relation was highlighted recently by the “raft hypothesis”. This hypothesis proposes that cell membranes laterally segregate into biologically relevant entities via phase separation mechanisms.<sup>40–52</sup> A variety of fluorescence approaches have been used to examine the existence and nature of lipid heterogeneities in biological membranes, including imaging of plasma membrane lipid heterogeneities,<sup>53,54</sup> fluorescence polarization studies,<sup>55</sup> fluorescence red shift imaging,<sup>56</sup> fluorescence resonance energy transfer imaging,<sup>57</sup> and single particle tracking.<sup>58</sup> The liquid-ordered phase (Lo) was considered as the putative “raft” phase coexisting with the liquid-disordered (Ld) phases. Some recent findings indicate that PAHs show a weak to pronounced affinity for Lo versus Ld phases.<sup>59</sup> The fact that the PAH excitation dipole moments in the Lo phase are oriented preferentially along the membrane normal is in accordance with PAHs intercalating into liquid-ordered membranes in a way similar to cholesterol, that is, by association of the flat PAH molecules with the hydrocarbon lipid chains.<sup>59</sup>

In this work, the effect of phenanthrene, anthracene, pyrene, chrysene, and benzo[a]pyrene on the model lipid membranes was studied. The monomolecular films formed on a pure water subphase with pure 1,2-dipalmitoyl-*sn*-glycero-3-phosphocholine (DPPC), 1,2-dipalmitoyl-*sn*-glycero-3-phosphoglycerol (DPPG),

1,2-dipalmitoyl-*sn*-glycero-3-phosphoserine (DPPS), 1,2-dipalmitoyl-*sn*-glycero-3-phosphoethanolamine (DPPE), 1,2-dimyristoyl-*sn*-glycero-3-phosphoethanolamine (DMPE), and cholesterol (CHOL) or mixed with PAHs were used as model membranes. The first four phospholipids allowed studying the effect of the polar head groups on the interactions with PAHs, while DMPE and cholesterol were used to study the effect of the chain length and structure of the nonpolar moiety of the lipid molecules. The interactions of PAHs with lipid monolayers were monitored via simultaneous measurements of surface pressure ( $\Pi$ ) and surface electrical potential ( $\Delta V$ ). Moreover, the morphology of the monolayers formed in the presence of PAHs was investigated using Brewster angle microscopy (BAM). Polarization-modulation infrared reflection–absorption spectroscopy (PM-IRRAS) was used to assess the interactions between PAHs and different moieties of the phospholipids. The orientation of PAHs in the monolayer was estimated based on modeling of PAH structure and on the parameters of the compression isotherms. The results obtained show that PAHs present in the monolayers have a meaningful impact on monolayer structure and properties.

Moreover, 1,2-dilauroyl-*sn*-glycero-3-phosphocholine (DLPC) was used in the experiments aiming at the enzymatic probing of the presence of a chosen PAH, namely, benzo[a]pyrene, in the monolayer. The choice of DLPC was dictated by the conditions of the enzymatic assay, in which water-insoluble substrates yielding water-soluble products have to be used. Interestingly, the presence of benzo[a]pyrene in the monolayers formed with DLPC does not affect the activity of phospholipase A2 (PLA<sub>2</sub>);<sup>60,61</sup> this lipolytic enzyme was used here as a tool for comparing the properties of the pure lipid monolayers and those containing PAHs. The latter observation suggests that the presence of PAHs in lipid membranes may go unnoticed for different enzymatic detoxification systems and that this could be the cause of their harmful effects.

## 2. Experimental Section

**Chemicals.** DPPC, DPPG, DLPC, DPPS, DPPE, DMPE, and cholesterol were from Sigma (phospholipids at least 95% pure; CHOL 99% pure). CaCl<sub>2</sub> was from Prolabo (purity 97%). Phenanthrene (98% pure), anthracene (at least 96% pure), pyrene (98% pure), chrysene (95% pure), and benzo[a]pyrene (at least 96% pure) were from Sigma; the latter molecules appear throughout the text in order of increasing area of the aromatic rings. MilliQ water used in the experiments contained between 6.1 and 21.7 ng mL<sup>−1</sup> (between 0.15 and 0.54 μM) of Ca<sup>2+</sup> cations, as determined using a Spectra AA 246 FS graphite furnace atomic absorption spectrometer (GFAAS; Varian, Palo Alto, CA). Spectrophotometric grade chloroform and methanol (Aldrich, A.C.S.) were used for preparing phospholipid and PAH solutions.

**Compression Isotherms and Brewster Angle Microscopy.** The surface pressure and electrical surface potential measurements were performed using a KSV 5000 Langmuir balance (KSV Instruments, Helsinki, Finland). A Teflon trough (15 cm × 58 cm × 1 cm) with two hydrophilic Delrin barriers (symmetric compression) was used in compression isotherm experiments. The system was equipped with an electrobalance and a platinum Wilhelmy plate (perimeter 39.24 mm) as a surface pressure sensor and a surface potential measuring head with a vibrating electrode. A platinum plate (4 cm diameter) immersed 4 mm below the water surface was used as a counter electrode. The apparatus was closed in a Plexiglas box, and the temperature was kept constant at 20 °C. Before each use, the

trough and the barriers were cleaned using cotton soaked in chloroform, gently brushed with ethanol and then with tap water and finally rinsed with MilliQ water. All solvents used for cleaning the trough and the barriers were of analytical grade. Aqueous subphases for monolayer experiments were prepared with MilliQ water, which had a surface tension of  $72.8 \text{ mN m}^{-1}$  at  $20^\circ\text{C}$ . Any residual surface-active impurities were removed before each experiment by sweeping and suction of the surface. Monolayers were spread using calibrated solutions with concentrations around  $1 \text{ mg mL}^{-1}$ . DPPC, DPPG, DLPC, and CHOL were dissolved in pure chloroform; DPPS, DPPE, and DMPE were dissolved in a chloroform/methanol 4:1 v/v mixture. The stock solutions of PAHs and lipids were used to prepare lipid/PAH mixtures with 9:1 molar ratio. The stability of the  $\Delta V$  signal was checked before each experiment, after cleaning the subphase surface. After the  $\Delta V$  signal had reached a constant value, it was zeroed and the film was spread on the subphase. After an equilibration time of 20 min, the films were compressed at a rate of  $2.5 \text{ mm min}^{-1} \text{ barrier}^{-1}$ . A personal computer equipped with KSV software was used to control the experiments. Each compression isotherm was performed at least three times. The standard error was  $\pm 0.5 \text{ \AA}^2$  with mean molecular area measurements and  $\pm 0.005 \text{ V}$  with surface potential measurements, respectively.

The morphology of the films was imaged with a computer-interfaced KSV 2000 Langmuir balance combined with a Brewster angle microscope (KSV Optrel BAM 300, KSV Instruments, Helsinki, Finland). The Teflon trough dimensions were  $6.5 \text{ cm} \times 58 \text{ cm} \times 1 \text{ cm}$ ; other experimental conditions were as described above.

**Polarization-Modulation Infrared Reflection-Absorption Spectroscopy.** The PM-IRRAS spectra of pure DPPE and mixed DPPE/benzo[a]pyrene monolayers spread on a pure water subphase were registered at  $20^\circ\text{C}$ . The Teflon trough dimensions were  $36.5 \text{ cm} \times 7.5 \text{ cm} \times 0.5 \text{ cm}$ ; other experimental conditions were as described in the preceding paragraph. The PM-IRRAS measurements were performed using a KSV PMI 550 instrument (KSV Instruments Ltd., Helsinki, Finland). The PMI 550 contains a compact Fourier transform IR spectrometer equipped with a polarization-modulation (PM) unit on one arm of a goniometer and a MCT detector on the other arm. The incident angle of the light beam can be freely chosen between 40 and  $90^\circ$ ; here, the incident angle was  $75^\circ$ . The spectrometer and the PM unit operate at different frequencies, allowing separation of the two signals at the detector. The PM unit consists of a photoelastic modulator, which is an IR-transparent, ZnSe piezoelectric lens. The incoming light is continuously modulated between *s*- and *p*-polarization at a frequency of 74 kHz. This allows simultaneous measurement of spectra for the two polarizations, the difference providing surface specific information and the sum providing the reference spectrum. As the spectra are measured simultaneously, the effect of water vapor is largely reduced. The half-wave retardation for modulation can freely be selected depending on the wavelength region of interest. The peak retardation wavelength used here was  $1500 \text{ cm}^{-1}$ . The spectral range of the device is  $800-4000 \text{ cm}^{-1}$ , and the resolution is  $8 \text{ cm}^{-1}$ .

**Enzymatic Lipolysis.** Porcine pancreatic phospholipase PLA<sub>2</sub> (EC.3.1.1.4; SIGMA, P6534; 1840 units  $\text{mg}^{-1}$ , conc.  $2.9 \text{ mg mL}^{-1}$ ) was used to catalyze the hydrolysis of DLPC. The lipolysis conditions were not optimized. The subphase was MilliQ water containing  $5 \text{ mM CaCl}_2$  (pH 5.8) or  $0.54 \mu\text{M Ca}^{2+}$  cations (pH 5.6). Benzo[a]pyrene was present in the lipid film spread as a DLPC/benzo[a]pyrene mixture with 9:1 molar

proportions. The experiments were performed with a KSV 5000 Langmuir balance (KSV, Helsinki) and a “zero order trough”<sup>62</sup> with symmetric compression. The experimental setup is described elsewhere.<sup>61</sup> The subphase was thermostatically maintained at  $20^\circ\text{C}$ . The enzyme solution was injected through the film with a Hamilton syringe ( $1 \mu\text{L}$  of the commercial enzyme solution). The final PLA<sub>2</sub> concentration in the subphase was  $66.7 \text{ units L}^{-1}$ . The surface pressure was maintained constant at  $10 \text{ mN m}^{-1}$  using the barostat technique.

### 3. Results and Discussion

#### Compression Isotherms and Brewster Angle Microscopy.

To address the question of the interactions between PAHs and lipid membranes, the interfacial properties of the mixed films formed with phenanthrene, anthracene, pyrene, chrysene, or benzo[a]pyrene (Figure 1) and phospholipids were studied at the air/water interface.

Three molecules, namely, anthracene (point group  $D_{2h}$ ), pyrene ( $D_{2h}$ ), and chrysene ( $C_{2h}$ ), have higher symmetry compared to phenanthrene ( $C_{2v}$ ) and benzo[a]pyrene ( $C_s$ ). As a consequence, the length as well as *x*, *y*, and *z* components of the dipole moment of the first three molecules are equal to zero, while the dipole moments of the last two molecules deviate from zero. The dipole moments of phenanthrene and benzo[a]pyrene are 0.038 and 0.042 D, respectively. The direction and orientation of both vectors are qualitatively shown in Figure 1. These data were obtained at the density functional level of theory [B3LYP/6-311G(d,p)].

The surface pressure-area ( $\Pi-A$ ) and surface potential-area ( $\Delta V-A$ ) isotherms obtained upon compression of pure DPPC, DPPE, DPPG, or DPPS and mixed lipid/PAH monolayers are shown in Figure 2. The monolayers were spread on the pure water subphase at  $20^\circ\text{C}$ .

The isotherms of pure phospholipids (Figure 2, black curves) resemble those published elsewhere.<sup>63,64</sup> At the maximal packing of the film, the isotherms show a solid state (S) with DPPE, DPPG, and DPPS and a liquid condensed phase (LC) with DPPC. All four phospholipid monolayers collapse at surface pressures of  $51.1-55.1 \text{ mN m}^{-1}$  and surface areas of  $36-43 \text{ \AA}^2$ . The maximum  $\Delta V$  values, corresponding to the maximum packing of molecules in the monolayer ( $\Delta V_{\max}$ ), with DPPC (0.56 V), DPPE (0.59 V), DPPG (0.25 V), and DPPS (0.30 V) are within the range reported in other papers.<sup>65,66</sup> The parameters of the collapse and the shape of the isotherms are modified upon the introduction of 10 mol %, of phenanthrene, anthracene, pyrene, chrysene, or benzo[a]pyrene in the phospholipid monolayers.

DPPC shows a LE-LC phase transition, which is absent in the other phospholipids. For this reason, DPPC is discussed separately from the other phosphoglycerides. The  $\Pi-A$  isotherms corresponding to the mixed DPPC/PAH monolayers (Figure 2A) are slightly shifted to higher molecular areas compared to the pure DPPC isotherm. The monolayers collapsed at almost the same area values but at different surface pressures (Table 1). The collapse pressures of DPPC/phenanthrene and DPPC/anthracene mixed films are higher compared to the collapse pressure of the pure DPPC, while an inverse tendency is observed for the other mixed films. The lowest collapse pressures, indicating a decrease of the monolayer stability, are observed with the DPPC/chrysene and DPPC/benzo[a]pyrene monolayers; in the latter case, it correlates with the  $\Delta V-A$  isotherm results, which show a low conformational phospholipid ordering in the mixed films.

All DPPC mixed films show a clear phase transition plateau. A small shift in the surface pressure of the phase transition

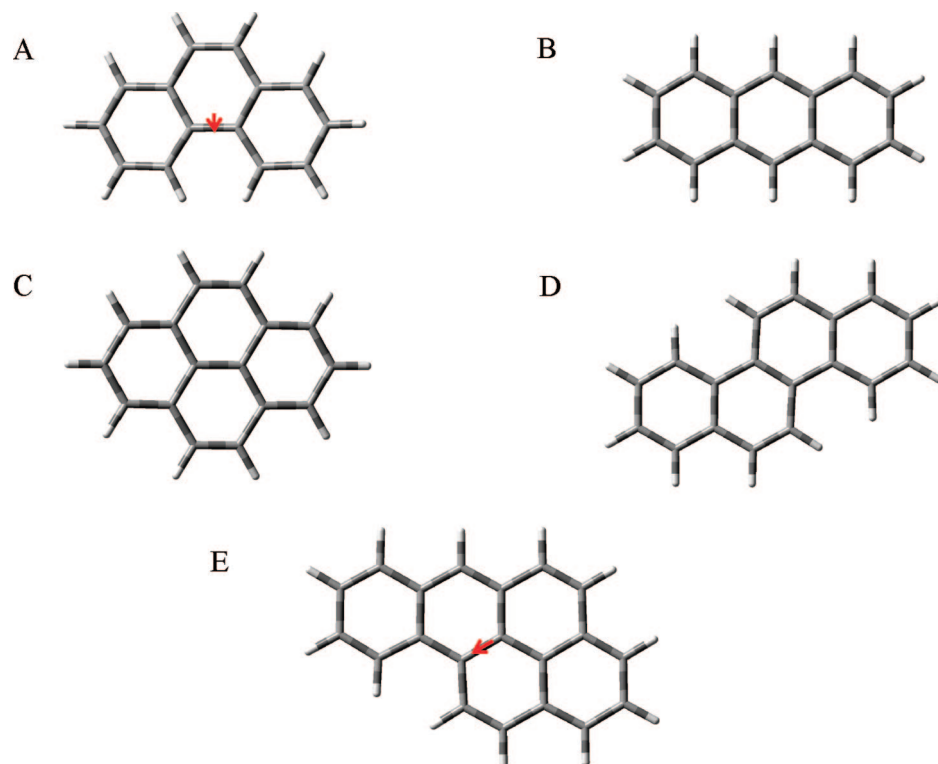


**Figure 1.** Models of phenanthrene (A), anthracene (B), pyrene (C), chrysene (D), and benzo[a]pyrene (E). The molecules are presented in the order of the increasing surface of the aromatic rings ( $72.0, 72.5, 78.0, 88.8$ , and  $94.8 \text{ \AA}^2$ ). The vectors of phenanthrene and benzo[a]pyrene dipole moments are indicated as red arrows.

region is observed with different mixtures. In the case of DPPC/pyrene, DPPC/anthracene, and DPPC/chrysene, and DPPC/benzo[a]pyrene monolayers, the LE-LC transition starts at a smaller area compared to the pure lipid monolayer. This effect is well visualized in the BAM micrographs presented in Figure 3. Indeed, the formation of the domains, typical for the DPPC phase transition, shows some modifications of the surface pressure and surface area values compared to the pure lipid. In the mixed DPPC/phenanthrene and DPPC/anthracene films, the lipid domains start to be visible at the surface pressure comparable to the pure DPPC monolayer, while, for the other mixed films, the domains appear at much higher surface pressures. In the presence of benzo[a]pyrene in the lipid film, the domain structure is different compared to those observed with the pure lipid film; the domains are small and dispersed in the LE phase (Figure 3Q). The BAM images of DPPC/chrysene monolayers (Figure 3M-O) indicate that chrysene is phase-separated from the phospholipid matrix and forms a distinct solid phase in the whole range of the experimental conditions.

At higher surface pressures, all monolayers become more condensed and at a surface pressure of  $30 \text{ mN m}^{-1}$ , which is relevant for biological membranes, the films are in a LC homogeneous phase. However, the condensation of DPPC/benzo[a]pyrene monolayer is lower, compared to the other mixed films. The lower film condensation in the LC phase together with the reduced size of the domains in the LE-LC transition in the presence of benzo[a]pyrene are in good agreement with a low compressibility modulus value ( $C_S^{-1}$ ;  $C_S^{-1} = -A(\partial\Pi/\partial A)_T$ ) calculated from the  $\Pi-A$  dependency<sup>67</sup> at the most condensed state of the monolayer (Table 1). Moreover, the  $C_S^{-1}$  values obtained from the DPPC/phenanthrene and DPPC/pyrene isotherms are in accordance with the BAM images. Indeed, the images indicate a more liquidlike character of the latter monolayers compared to those formed with the pure DPPC and DPPC/anthracene mixture.

The DPPE/PAH, DPPG/PAH, and DPPS/PAH isotherms are presented in parts B, C, and D of Figure 2, respectively, and their characteristic parameters are given in Table 1. As shown in Figure 2B-D, the  $\Pi-A$  isotherms corresponding to the mixed films are shifted to higher molecular areas compared to the pure lipid isotherms. The isotherm shift is more pronounced in the case of DPPE and DPPS, compared to the DPPG film. The molecular areas at the collapse of the monolayers increase by  $1-4 \text{ \AA}^2$  above the value of the pure lipids, while the stability of the monolayers decreases, as indicated by the decreasing values of  $\Pi_{\text{collapse}}$ . The lowest stability of the films is observed with the monolayers containing benzo[a]pyrene. Interestingly, in the case of the DPPE matrix, the low stability and high monolayer fluidization reflected by the  $C_S^{-1}$  values is accompanied by a decrease of the  $\Delta V_{\text{max}}$  value. These results may be linked to a lower ordering of the molecules in the DPPE film containing benzo[a]pyrene compared to other PAHs, as was observed in the case of DPPC. This effect is particularly well seen in the profile of the benzo[a]pyrene  $\Delta V-A$  isotherm (Figure 2 B), for which takeoff is shifted to the lowest molecular area values compared to other PAHs. On the contrary, the DPPS/benzo[a]pyrene mixture shows a higher  $\Delta V_{\text{max}}$  value compared to that of the pure phospholipid and a monotonic overall rise of the  $\Delta V-A$  isotherm. This result may be linked to the dipole-dipole interactions between the negatively charged phospholipid and benzo[a]pyrene, having a small dipole moment, as calculated theoretically. It can be noticed that a small (within the error limits) increase in the surface potential value is also observed in the case of the DPPS/phenanthrene monolayers. The changes in the molecular area values induced by phenanthrene, anthracene, pyrene, and chrysene incorporated in the DPPG matrix (Figure 2C and Table 1) are small, although the monolayers collapse at different surface pressures. The isotherm parameters show that the phospholipid monolayer containing anthracene is the most stable, condensed, and ordered,

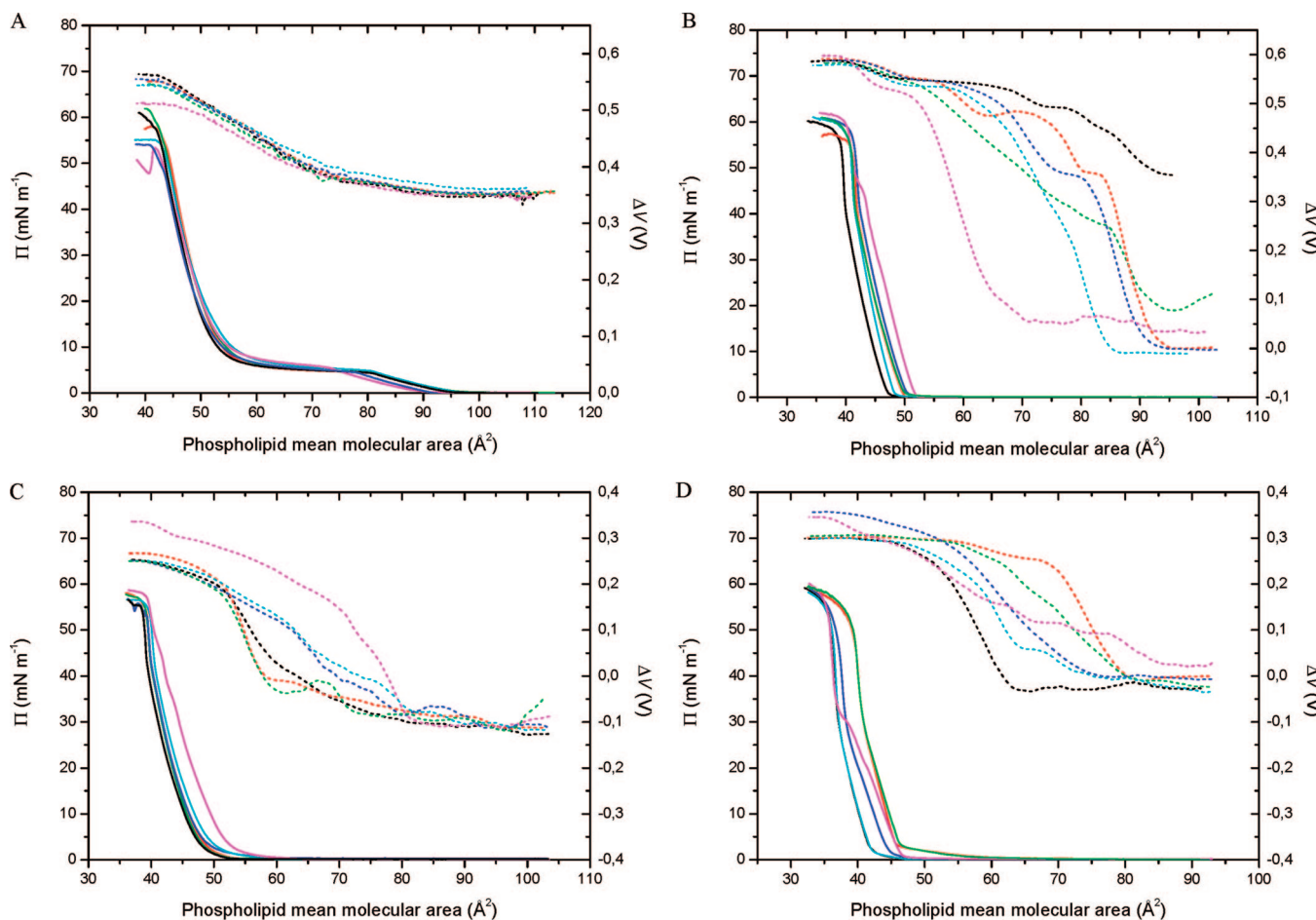


**Figure 2.** Compression isotherms of phospholipid monolayers spread in the presence and in the absence of PAHs. Results obtained with (A) DPPC, (B) DPPE, (C) DPPG, and (D) DPPS. Solid lines,  $\Pi$ - $A$  isotherms; dashed lines,  $\Delta V$ - $A$  isotherms. Black curves, pure lipid film; green curves, mixed lipid/phenanthrene film; red curves, mixed lipid/anthracene film; cyan curves, mixed lipid/pyrene film; blue curves, mixed lipid/chrysene film; magenta curves, mixed lipid/benzo[a]pyrene film. Subphase: pure water; temperature 20 °C.

**TABLE 1: Parameters of Pure Lipid and Mixed Lipid/PAHs Monolayers**

	$\Pi_{\text{collapse}}$ ( $\text{mN m}^{-1}$ )	$A_{\text{collapse}}$ ( $\text{\AA}^2$ )	$C_S^{-1}$ ( $\text{mN m}^{-1}$ )	$\Delta V_{\text{max}}$ (V)
DPPC	53.8	43	300.2	0.56
DPPC/phenanthrene	54.8	43	314.6	0.54
DPPC/anthracene	54.3	44	307.8	0.55
DPPC/pyrene	53.3	43	286.7	0.54
DPPC/chrysene	47.9	43	271.8	0.55
DPPC/benzo[a]pyrene	49.0	43	241.7	0.51
DPPE	55.1	39	1131.6	0.59
DPPE/phenanthrene	53.6	42	986.5	0.58
DPPE/anthracene	53.4	40	1012.3	0.59
DPPE/pyrene	54.3	41	984.1	0.58
DPPE/chrysene	54.7	41	854.6	0.59
DPPE/benzo[a]pyrene	44.0	43	485.7	0.58
DPPG	53.5	39	876.5	0.25
DPPG/phenanthrene	53.2	39	823.4	0.25
DPPG/anthracene	54.1	39	1023.4	0.26
DPPG/pyrene	53.5	40	775.7	0.25
DPPG/chrysene	52.9	39	804.3	0.25
DPPG/benzo[a]pyrene	36.0	39	343.7	0.38
DPPS	51.1	36	1022.6	0.30
DPPS/phenanthrene	46.9	40	797.7	0.31
DPPS/anthracene	46.6	40	795.0	0.30
DPPS/pyrene	49.1	36	953.6	0.30
DPPS/chrysene	46.4	37	672.3	0.36
DPPS/benzo[a]pyrene	29.3	39	197.4	0.32

while that containing benzo[a]pyrene is the most liquidlike and the least stable. A significantly higher surface potential value is observed with the DPPG/benzo[a]pyrene compared to the

other PAHs. The latter supports our proposal that benzo[a]pyrene and the negatively charged phospholipids establish dipole-dipole interactions, which contribute to the overall  $\Delta V$  value. The results obtained with the compression experiments reveal differences between benzo[a]pyrene and other PAHs. Indeed, the monolayers containing benzo[a]pyrene are less stable and more liquidlike compared to those containing the other PAHs. It cannot be excluded that these differences account for the higher toxicity of benzo[a]pyrene observed *in vivo*.

The BAM micrographs support the conclusions coming from the analysis of the compression isotherms. The BAM images of pure DPPE, DPPG, or DPPS and lipid/PAH mixed monolayers are presented in Figures 4, 5, and 6, respectively. The first column corresponds to the LE-G phase transition at  $\Pi$  around 0  $\text{mN m}^{-1}$ , while the second one, to the condensed monolayer at  $\Pi = 30 \text{ mN m}^{-1}$ . As shown in the DPPC micrographs, chrysene does not mix with the other lipids and forms a separate crystal phase in the DPPE, DPPG, and DPPS matrices, which is well visualized in both states of the monolayer (snapshots E and K). The differences in the condensation of mixed films are clearly visible in the images taken in the LE-G phase transition. In general, the presence of PAHs induces a more liquidlike character of the phospholipid films. The film fluidization is low or it does not show in the presence of anthracene, while it increases in the case of other PAHs; the latter correlates well with the compressibility modulus values. The condensed films are isotropic with all PAHs except the

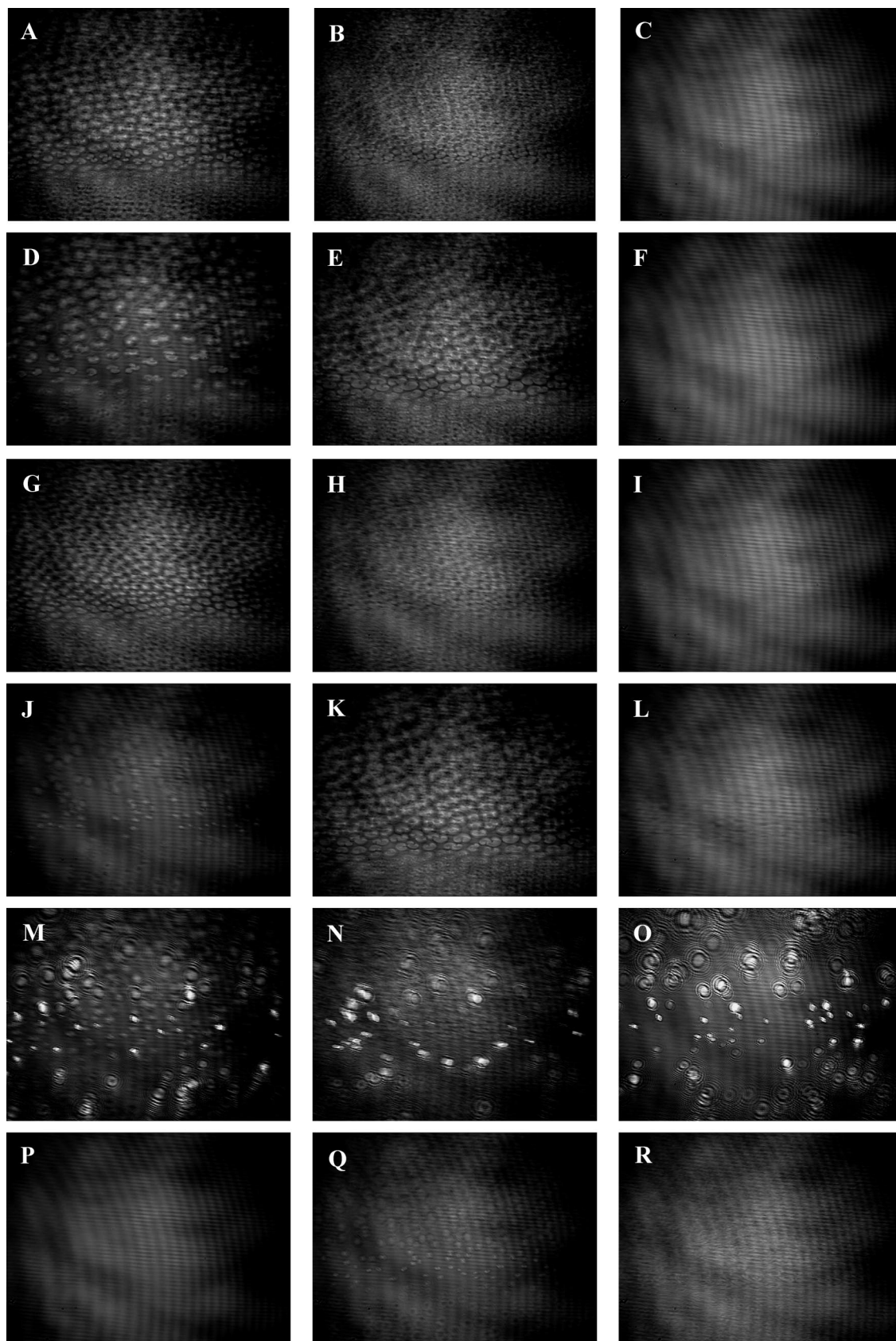


**Figure 3.** Brewster angle micrographs of DPPC and DPPC/PAH monolayers. (A–C) BAM micrographs of pure DPPC monolayer; (D–F) DPPC/phenanthrene, (G–I) DPPC/anthracene, (J–L) DPPC/pyrene, (M–O) DPPC/chrysene, and (P–R) DPPC/benzo[a]pyrene mixtures. The micrographs (A, D, G, J, M, P) were taken at  $\Pi = 5.0 \text{ mN m}^{-1}$ ; (B, E, H, K, N, Q)  $6.0 \text{ mN m}^{-1}$ ; and (C, F, I, L, O, R)  $30.0 \text{ mN m}^{-1}$ . Scale: the width of the snapshots corresponds to  $400 \mu\text{m}$ .

highly compressible mixtures containing benzo[a]pyrene. Indeed, the micrographs of DPPE/benzo[a]pyrene (Figure 4L) or

DPPG/benzo[a]pyrene (Figure 5L) monolayers show anisotropic patterns. In the case of the DPPS/benzo[a]pyrene system (Figure

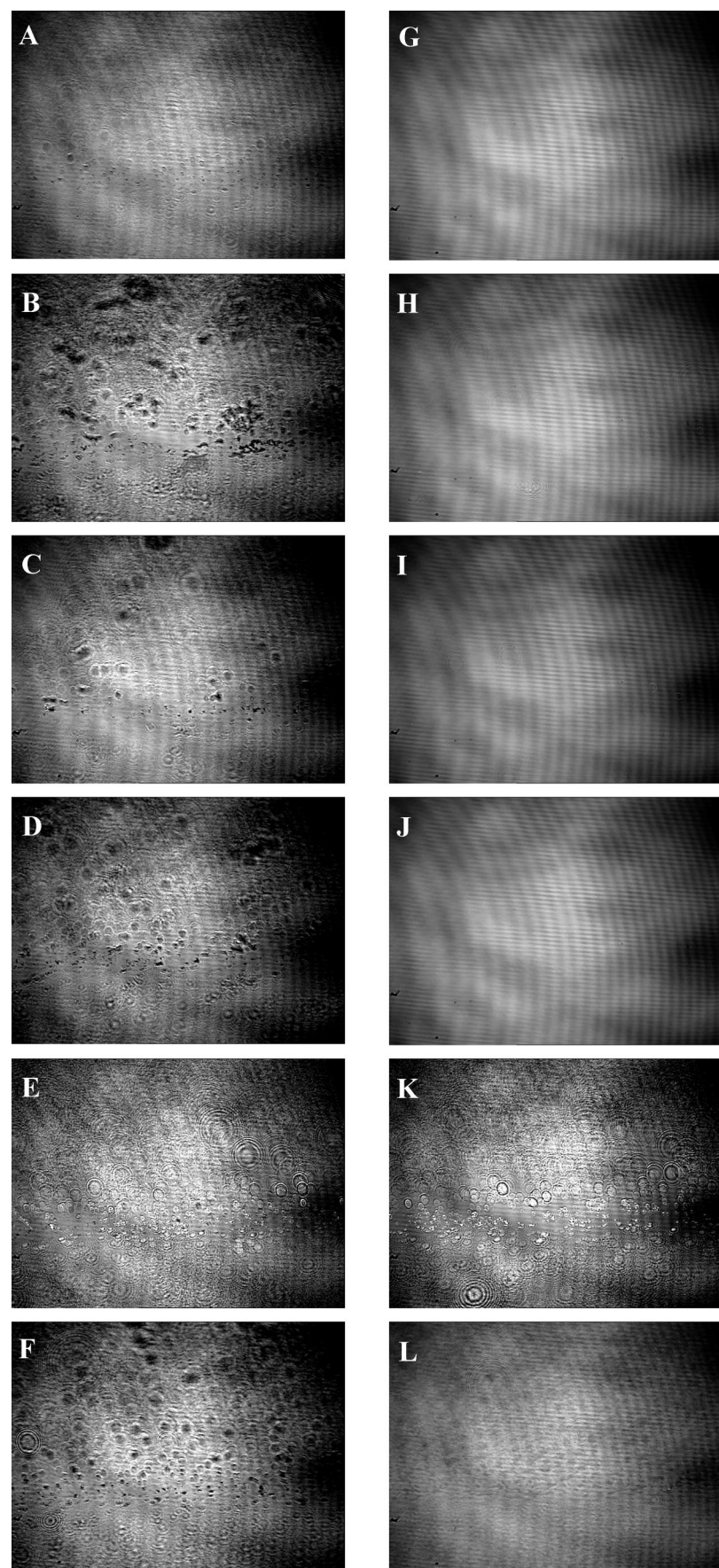


**Figure 4.** Brewster angle micrographs of DPPE and DPPE/PAHs monolayers. (A, G) BAM micrographs of pure DPPE monolayer; (B, H) DPPE/phenanthrene, (C, I) DPPE/anthracene, (D, J) DPPE/pyrene, (E, K) DPPE/chrysene, and (F, L) DPPE/benzo[a]pyrene mixtures. The micrographs were taken at  $\Pi = 0 \text{ mN m}^{-1}$ ,  $A = 70 \text{ \AA}^2$  (A–F) and  $30.0 \text{ mN m}^{-1}$  (G–L). Scale: the width of the snapshots corresponds to  $400 \mu\text{m}$ .

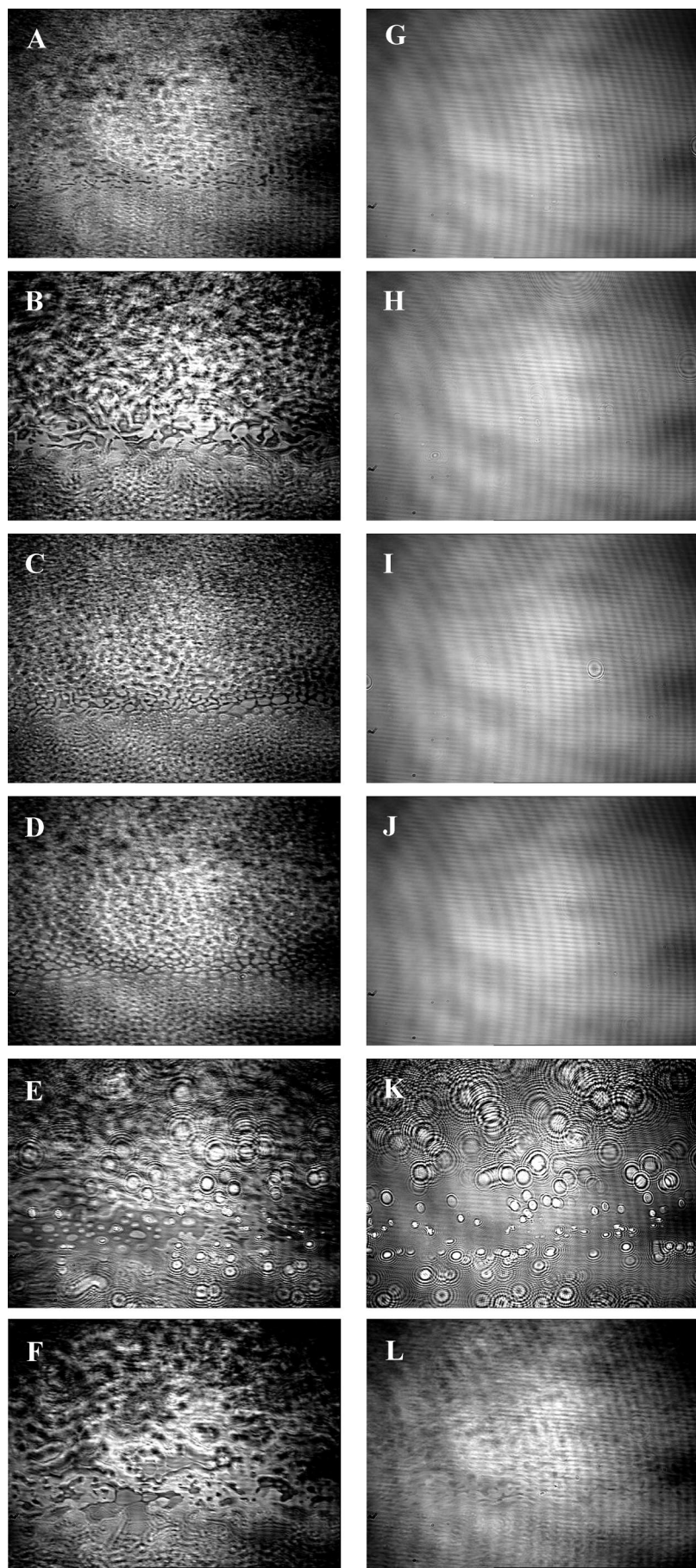


**Figure 5.** Brewster angle micrographs of DPPG and DPPG/PAH monolayers. (A, G) BAM micrographs of pure DPPG monolayer; (B, H) DPPG/phenanthrene, (C, I) DPPG/anthracene, (D, J) DPPG/pyrene, (E, K) DPPG/chrysene, and (F, L) DPPG/benzo[a]pyrene mixtures. The micrographs were taken at  $\Pi = 0 \text{ mN m}^{-1}$ ,  $A = 70 \text{ \AA}^2$  (A–F) and  $30.0 \text{ mN m}^{-1}$  (G–L). Scale: the width of the snapshots corresponds to  $400 \mu\text{m}$ .

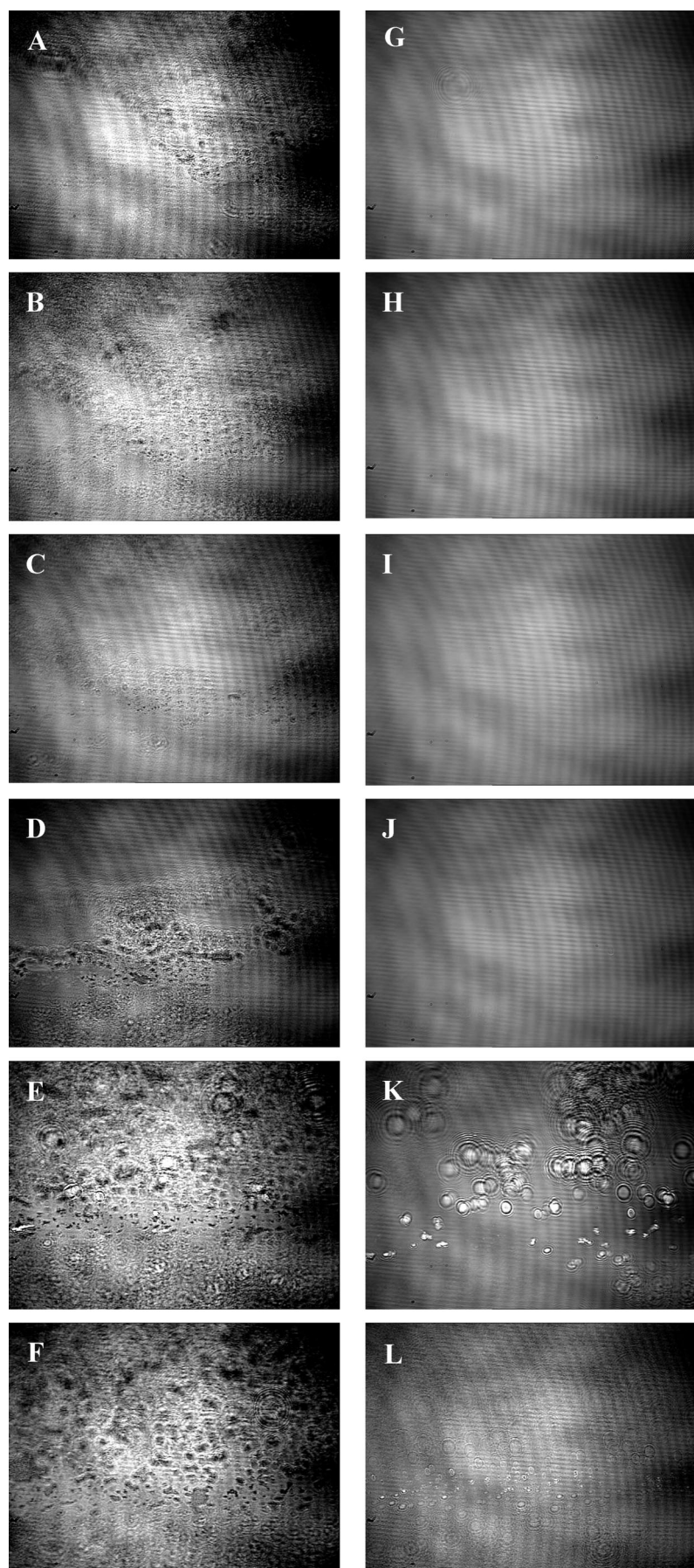


**Figure 6.** Brewster angle micrographs of DPPS and DPPS/PAH monolayers. (A, G) BAM micrographs of pure DPPS monolayer; (B, H) DPPS/phenanthrene, (C, I) DPPS/anthracene, (D, J) DPPS/pyrene, (E, K) DPPS/chrysene, and (F, L) DPPS/benzo[a]pyrene mixtures. The micrographs were taken at  $\Pi = 0 \text{ mN m}^{-1}$ ,  $A = 60 \text{ \AA}^2$  (A–F) and  $30.0 \text{ mN m}^{-1}$  (G–L). Scale: the width of the snapshots corresponds to  $400 \mu\text{m}$ .

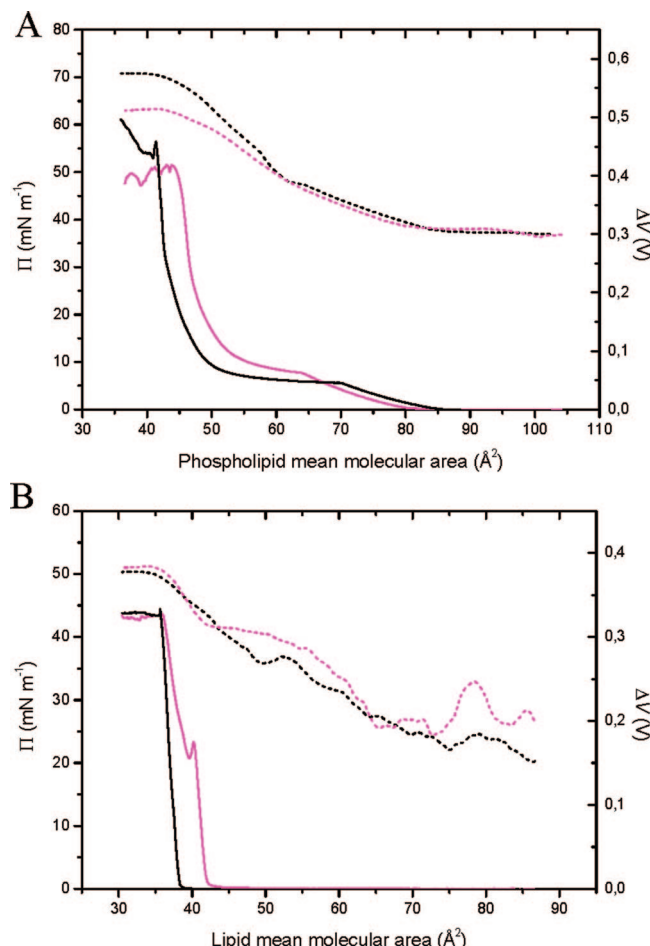


**Figure 7.** Compression isotherms of (A) DMPE and (B) CHOL monolayers spread in the presence and in the absence of benzo[a]pyrene. Solid lines,  $\Pi$ - $A$  isotherms; dashed lines,  $\Delta V$ - $A$  isotherms. Black curves, pure lipid film; magenta curves, mixed lipid/benzo[a]pyrene film. Subphase: pure water; temperature 20 °C.

**TABLE 2: Parameters of Pure CHOL and DMPE and Mixed Monolayers**

	$\Pi_{\text{collapse}}$ (mN m <sup>-1</sup> )	$A_{\text{collapse}}$ (Å <sup>2</sup> )	$C_S^{-1}$ (mN m <sup>-1</sup> )	$\Delta V_{\text{max}}$ (V)
DMPE	55.8	42	909.2	0.58
DMPE/benzo[a]pyrene	47.3	45	702.1	0.53
CHOL	44.4	36	964.9	0.37
CHOL/benzo[a]pyrene	23.3	40	697.5	0.34

6L), the micrograph corresponds to the collapsed film, showing as a condensed phospholipid matrix with imbedded small solid crystals.

To get more insight into the influence of PAHs on the lipid membrane structure and properties, the investigations were extended to a medium length chain DMPE and cholesterol (CHOL). The compression isotherms obtained with DMPE and CHOL are shown in parts A and B of Figure 7, respectively. The isotherm parameters are given in Table 2.

With both lipids, the molecular areas measured at the collapse of the mixed monolayers are significantly higher compared to the pure lipids, indicating the incorporation of benzo[a]pyrene into the lipid matrix. The lower values of the surface pressure as well as the compressibility modulus indicate that the mixed films become more liquid and less stable compared to the pure films. The decrease in the surface potential values suggests a lower ordering of the molecules in the film. The BAM micrographs of DMPE/benzo[a]pyrene mixed film (Figure

8D–F) indicate that benzo[a]pyrene affects the size and structure of the LE–LC phase transition domains of the lipid; the domains are smaller and less branched compared to the LC domains in the pure DMPE film. Moreover, the domains appear at higher surface pressures compared to the pure lipid film, which is in agreement with the shift of the phase transition to higher pressures observed in the  $\Pi$ - $A$  isotherm. In the case of the CHOL/benzo[a]pyrene system, the fluidization of the monolayer is not visualized with BAM. At low surface pressures, the structure of the mixed monolayer corresponding to the LE–G phase transition (Figure 8J) is more homogeneous compared to the pure CHOL film. At 30 mN m<sup>-1</sup>, small bright spots in the condensed lipid matrix appear, indicating the immiscibility of benzo[a]pyrene with CHOL at high surface pressures. The  $\Pi$ - $A$  isotherm shows a sharp kink at 23.3 mN m<sup>-1</sup>; above this point, the isotherm of the mixed film approaches the isotherm of the pure CHOL. The latter observations indicate phase separation, which is in accordance with the results obtained with BAM. It can be noticed that the DPPS/benzo[a]pyrene yielded  $\Pi$ - $A$  isotherms with profiles similar to those of the CHOL/benzo[a]pyrene films.

The results obtained with the surface pressure isotherms were used to estimate the orientation of the PAH molecules in the lipid monolayers. The maximal surface of the phenanthrene, anthracene, pyrene, chrysene, and benzo[a]pyrene aromatic rings obtained with molecular modeling is, respectively, 72.0, 72.5, 78.0, 88.8, and 94.8 Å<sup>2</sup>; the maximal/minimal surfaces of the projections of these molecules on a plane perpendicular to the plane of the aromatic rings are, respectively, 39.2/26.4, 40.5/23.6, 39.8/30.3, 46.8/26.8, and 45.9/31.4 Å<sup>2</sup>. The comparison of the molecular areas at the collapse of the pure lipid and mixed monolayers with the molecular areas of PAHs in different projections let us speculate about the orientation of the PAHs in the monolayers. It can be observed that the molecular areas at the collapse are higher than those corresponding to 10 mol % of PAHs with the long molecule axis oriented vertically in the film but lower compared to PAHs laying flat on the water surface. On the basis of this observation, we propose that PAHs are intercalated between the phospholipid hydrocarbon chains, with the aromatic ring plane tilted relative to the water plane; the tilt would be different for different PAHs and phospholipids. In the case of phenanthrene and benzo[a]pyrene, the small dipole moment vector laying in the plane of the aromatic rings indicates that these molecules are oriented nonhorizontally relative to the water plane. The most important increase of the molecular area at the collapse is observed in the case of the lipids with small polar heads, namely, DPPE, DPPS, DMPE, and CHOL, compared to the lipids with bulky polar heads, namely, DPPC and DPPG. The latter may indicate that PAHs occupy voids between the hydrocarbon chains in the films formed with DPPC and DPPG, while DPPE, DPPS, DMPE, and CHOL are pushed aside by the inserted PAHs. To understand better the interactions between PAHs and the phospholipids, PM-IRRAS in monolayers was performed.

**Polarization-Modulation Infrared Reflection–Absorption Spectroscopy.** The DPPE/benzo[a]pyrene system was chosen to perform the PM-IRRAS experiments. The normalized spectra acquired in the monolayers spread at the air/water interface at 30 mN m<sup>-1</sup> are presented in Figure 9. Some differences can be seen in the spectra of the pure DPPE and mixed DPPE/benzo[a]pyrene films. The peaks corresponding to the methylene symmetric and asymmetric stretching in the DPPE hydrocarbon chains<sup>68</sup> appear at  $\nu_s(\text{CH}_2) \sim 2851 \text{ cm}^{-1}$  and  $\nu_{as}(\text{CH}_2) \sim 2921 \text{ cm}^{-1}$  in both spectra. However, the  $\sim 1724 \text{ cm}^{-1}$  peak corre-

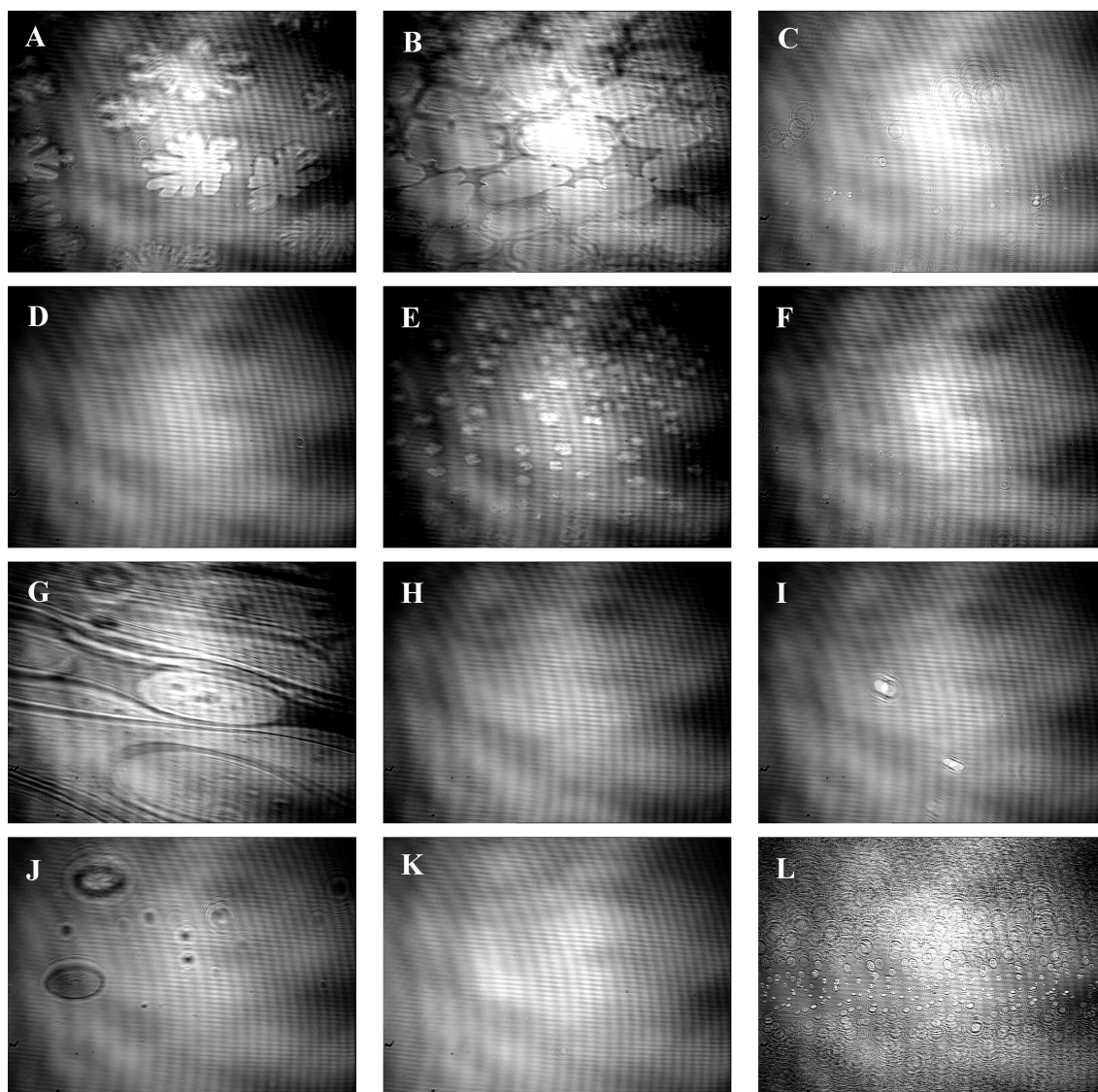


**Figure 8.** Brewster angle micrographs of DMPE (A–C), DMPE/benzo[a]pyrene (D–F), CHOL (G–I), and CHOL/benzo[a]pyrene (J–L) monolayers. The micrographs (A, D) were taken at  $\Pi = 6 \text{ mN m}^{-1}$ ; (B, E)  $8 \text{ mN m}^{-1}$ ; (G, J)  $\Pi = 0 \text{ mN m}^{-1}$ ,  $A = 80 \text{ \AA}^2$ ; (H, K)  $\Pi = 10 \text{ mN m}^{-1}$ ; and (C, F, I, L)  $30.0 \text{ mN m}^{-1}$ . Scale: the width of the snapshots corresponds to  $400 \mu\text{m}$ .

sponding to the DPPE carbonyl symmetric stretching is shifted to  $\sim 1737 \text{ cm}^{-1}$  in the mixed DPPE/benzo[a]pyrene film. This effect could be explained by breaking the hydrogen bonding between water and the DPPE carbonyl groups<sup>69–72</sup> in the presence of the intercalated benzo[a]pyrene molecules. The latter suggests in turn that the benzo[a]pyrene molecules are lodged close to the lipid polar head region. This proposal is in accordance with the expanding effect observed with the  $\Pi-A$  compression isotherms in the DPPE/benzo[a]pyrene films and, on the other hand, with our proposal of the interactions between benzo[a]pyrene and the polar moieties of the phospholipid.

**Enzymatic Probing of the PAH Effect.** Under physiological conditions, phospholipids undergo hydrolytic degradation catalyzed by lipolytic enzymes, phospholipases. Lipolytic enzymes are known to be active on the aggregated forms of their lipid substrates<sup>73–77</sup> and to depend in their activity and specificity on the physicochemical properties of the aggregate surface.<sup>78–80</sup> Here, PLA<sub>2</sub> was used as a probe differentiating between the phospholipid monolayers in the presence and in the absence of benzo[a]pyrene. In these experiments, 1,2-dilauroyl-*sn*-glycerol-3-phosphocholine (DLPC) was chosen as a model substrate, as the reaction products are water-soluble; the latter is the

prerequisite for monitoring the enzyme action using the monomolecular film technique.<sup>81–83</sup> Since PLA<sub>2</sub> is a calcium dependent enzyme,<sup>76,84,85</sup> the reactions were performed in the presence of Ca<sup>2+</sup> cations in the subphase. To evaluate the influence of Ca<sup>2+</sup> on the properties of the DLPC monolayer, the  $\Pi-A$  compression isotherms were performed on the pure water (i.e., MilliQ water containing trace quantities of Ca<sup>2+</sup> cations, as determined with GFAAS) and on the 5 mM CaCl<sub>2</sub> solution (Figure 10). It can be observed that the presence of 5 mM CaCl<sub>2</sub> in the subphase does not influence the isotherm profile.

As indicated by the shift of the  $\Pi-A$  isotherms, the DLPC/benzo[a]pyrene monolayer is slightly expanded compared to the pure DLPC. It is interesting to notice that the expanding effect of benzo[a]pyrene disappears in the presence of cholesterol, which has a clearly visible condensing effect on the phospholipid monolayer.<sup>67</sup> Importantly, as indicated by the  $\Delta V-A$  isotherms, the overall orientation of the molecules forming the mixed DLPC/benzo[a]pyrene as well as DLPC+CHOL/benzo[a]pyrene films is less vertical compared to pure DLPC. Obviously, the overall tilting of the molecules is induced both by cholesterol

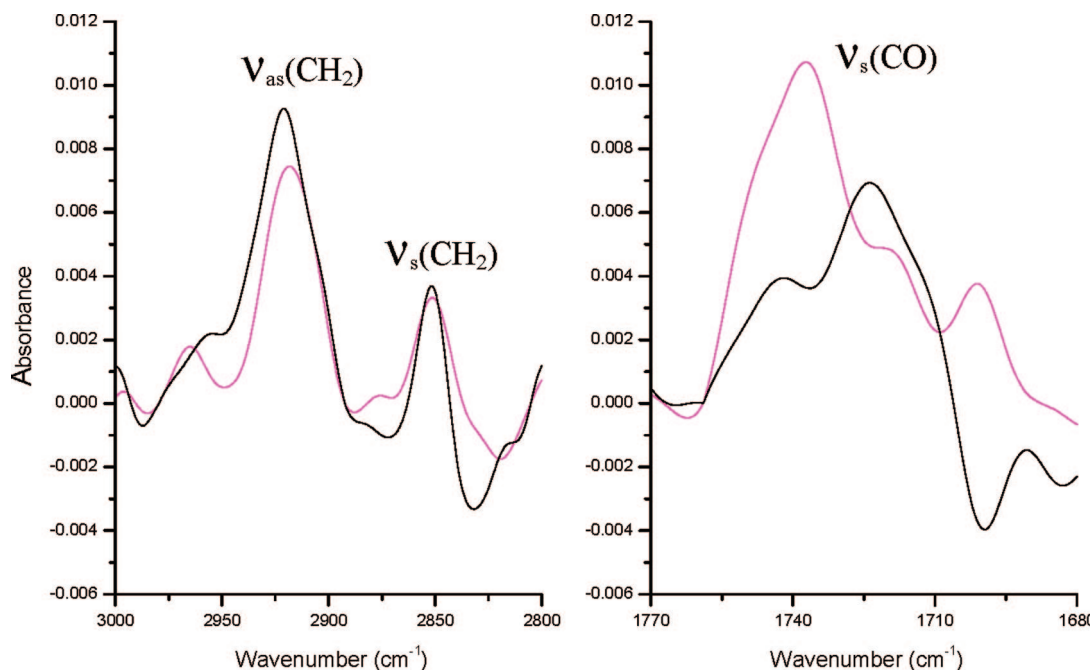


**Figure 9.** PM-IRRAS spectra of the pure DPPE (black curve) and mixed DPPE/benzo[a]pyrene monolayers (magenta curve) spread on the pure water subphase. Surface pressure 30 mN  $\text{m}^{-1}$ ; temperature 20 °C.

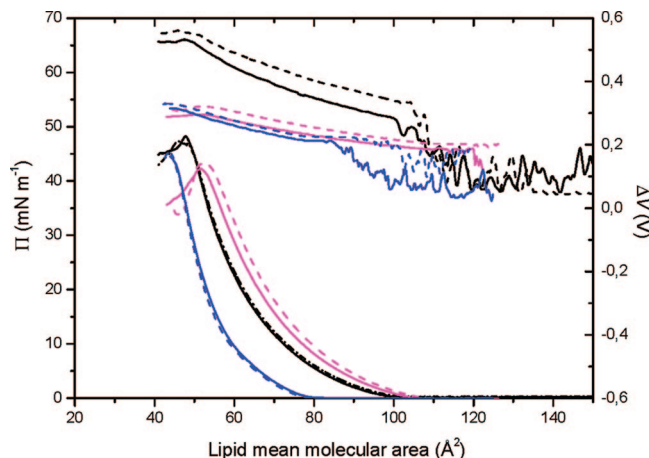


**Figure 10.** Compression isotherms of DLPC (black curves), DLPC/benzo[a]pyrene 9:1 (magenta curves), and (DLPC+CHOL)/benzo[a]pyrene 9:1 (blue curves) films spread on a pure water subphase (solid lines) and 5 mM CaCl<sub>2</sub> (dashed lines). Temperature 20 °C.

and by benzo[a]pyrene, and independent of the respective condensing or expanding effects of these molecules.

Interestingly, the differences of the film properties observed with the compression isotherms are not reflected in the activity of PLA<sub>2</sub>. Indeed, in the presence of 5 mM CaCl<sub>2</sub> in the subphase, the reaction rates observed with the DLPC or DLPC/CHOL films, as well as those containing benzo[a]pyrene, are close (Figure 11). The specific activity of PLA<sub>2</sub> is around 0.4  $\mu\text{mol min}^{-1} \text{mg}^{-1}$  with all of the substrates used. In the presence of trace amounts of CaCl<sub>2</sub> in the subphase, no activity of the phospholipase was detected, either with pure DLPC or with mixed DLPC/benzo[a]pyrene monolayers. It was observed recently that the presence of an antibiotic, griseofulvin, in the DLPC film influenced the activity of PLA<sub>2</sub>.<sup>61</sup> It was proposed that the amphiphilic griseofulvin intercalated between the phospholipid polar heads interferes in the process of the adsorption of the enzyme to the film. The results obtained in this work show that the aromatic molecules intercalated between the phospholipid hydrocarbon chains do not influence the

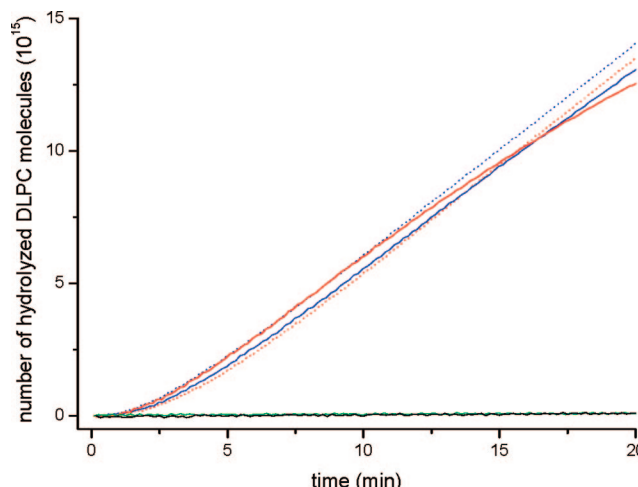


**Figure 11.** Hydrolysis of DLPC catalyzed by PLA<sub>2</sub>. The enzymatic lipolysis of the DLPC monolayer was performed at an arbitrarily chosen surface pressure of 10 mN  $\text{m}^{-1}$ . Red and blue curves, 5 mM CaCl<sub>2</sub> aqueous subphase; black and green curves, pure water subphase; blue dotted curve, pure DLPC; blue solid curve, DLPC/CHOL 7:3; red dotted curve, DLPC/benzo[a]pyrene 9:1; red solid curve, (DLPC+CHOL)/benzo[a]pyrene 9:1; black curve, pure DLPC; green curve, DLPC/benzo[a]pyrene 9:1. The concentration of Ca<sup>2+</sup> cations measured in pure water with GFAAS was 21.7 ng  $\text{mL}^{-1}$  (0.54  $\mu\text{M}$ ) in MilliQ water used in the experiments.

catalytic process. It can be supposed that the adsorption of the enzyme to the film occurs in the same way on the pure DLPC films and on the films containing polycyclic CHOL or benzo[a]pyrene, as cholesterol and PAHs are imbedded in the hydrophobic region of the film and do not interact directly with the enzyme. Along this line, PLA<sub>2</sub> could be considered as a probe detecting the position of different molecules in the membranes formed with the lipids, which are the enzyme's substrates. The latter proposal should be checked with a number of molecules of different polarity.

#### 4. Conclusions

The toxicity of PAHs is structurally dependent, with isomers varying from being nontoxic to being extremely toxic.<sup>3</sup> Among the five PAHs studied here, only benzo[a]pyrene and chrysene are known as toxic, namely, carcinogenic, mutagenic, and teratogenic. Interestingly, these two molecules have the biggest surface of the aromatic rings and are the most voluminous, as shown here with molecular modeling. It was observed that the biological effects of PAHs are often mediated by oxidative metabolism of the parent hydrocarbon to reactive intermediates that adduct DNA and induce oxidative stress.<sup>86</sup> The direct interactions of PAHs with lipid membranes may as well lead to biological effects by modifying the essential membrane parameters.<sup>87</sup> Here, we show that the presence of 10 mol % PAHs in the model membranes influences significantly their structure and physicochemical properties. Indeed, PAHs modify the phase transitions in the films and the morphology of the domains; the monolayers are more expanded in the presence of PAHs and, with the exception of the DPPG/anthracene, DPPC/anthracene, and DPPC/phenanthrene, more liquidlike. Among the PAHs studied, benzo[a]pyrene, which is the biggest molecule used here, yields the most notable effects. On the other hand, the compression experiments indicate that the PAHs imbedded between the lipid molecules acquire a tilted orientation; PM-IRRAS results indicate that benzo[a]pyrene interacts with the carbonyl groups of the phospholipid polar heads. The results obtained with the monolayer hydrolysis catalyzed by PLA<sub>2</sub> suggest that benzo[a]pyrene is not accessible to the enzyme. The overall results indicate that benzo[a]pyrene is lodged between and interacts with the hydrocarbon and carbonyl groups of the phospholipids and does not protrude from the monolayer. In conclusion, we propose that two different effects may contribute to PAH toxicity. First, the low quantities of PAHs embedded in biological membranes could be dissimulated from the action of different detoxification systems. Second, the modification of the lipid membrane properties may induce disturbance in the functioning of different membrane protein systems.

**Acknowledgment.** B.K. acknowledges a three-month fellowship from Nancy Université. We thank Dr. Eric Meux and Dr. Sébastien Déliberto, Laboratoire d'Electrochimie des Matériaux, UMR CNRS 7555, Université de Metz, for graphite furnace atomic absorption spectrometry trace analysis. We thank Dr. Jacek Korchowiec (Jagiellonian University, Krakow, Poland), Dr. Jorma Vuorinen, and Dr. Sauli Törmälä (KSV, Finland) for fruitful discussions. We thank Dr. Matthew Fielden (KSV, Finland) for correcting the English.

#### References and Notes

- (1) <http://www.health.state.mn.us/divs/eh/risk/guidance/pahmemo.html>.
- (2) <http://www.atsdr.cdc.gov/toxprofiles/phs69.html>.
- (3) *Toxicological Profile for Polycyclic Aromatic Hydrocarbons*; U.S. Dept. Health & Human Services: Atlanta, GA, 1995.
- (4) Kallimanis, A.; Frillingos, S.; Drainas, C.; Koukkou, A. I. *Appl. Microbiol. Biotechnol.* **2007**, *76*, 709–717.
- (5) Kanaly, R. A.; Harayama, S. *J. Bacteriol.* **2000**, *182*, 2059–2067.
- (6) Eisler, R. Patuxent Wildl. Res. Cent., Laurel, MD, 1987; pp 93.
- (7) Kim, Y. S.; Min, J.; Hong, H. N.; Park, J. H.; Park, K. S.; Gu, M. B. *Chemosphere* **2007**, *66*, 1243–1248.
- (8) <http://www.epa.gov/R5Super/ecology/html/toxprofiles.htm#pahs>.
- (9) *Toxicological Profile for Polycyclic Aromatic Hydrocarbons (PAHs) Draft Update*; U.S. Dept. Health & Human Services, 1993.
- (10) de Maagd, P. G.-J.; Ten Hulscher, D. T. E. M.; Van den Heuvel, H.; Opperhuizen, A.; Sijm, D. T. H. M. *Environ. Toxicol. Chem.* **1998**, *17*, 251–257.
- (11) Wang, L.; Srivastava, P.; Govind, R. AIChE Annual Meeting, Conference Proceedings, Cincinnati, OH, Oct. 30–Nov. 4, 2005, 143ab/141–143ab/117.
- (12) Grova, N.; Feidt, C.; Laurent, C.; Rychen, G. *Int. Dairy J.* **2002**, *12*, 1025–1031.
- (13) Laurent, C.; Feidt, C.; Lichtfouse, E.; Grova, N.; Laurent, F.; Rychen, G. *J. Agric. Food Chem.* **2001**, *49*, 2493–2496.
- (14) Lapole, D.; Monteau, F.; Grova, N.; le Bizec, B.; Rychen, G.; Feidt, C. *J. Dairy Sci.* **2007**.
- (15) Cavret, S.; Feidt, C.; Laurent, F. *J. Agric. Food Chem.* **2005**, *53*, 2773–2777.
- (16) Cavret, S.; Feidt, C.; Le Roux, Y.; Laurent, F. *J. Dairy Sci.* **2005**, *88*, 67–70.
- (17) Overton, E. *Vierteljahrsschr. Naturforsch. Ges. Zürich* **1899**, *44*, 88–114.
- (18) Bemporad, D.; Essex, J. W.; Luttmann, C. *J. Phys. Chem. B* **2004**, *108*, 4875–4884.
- (19) Beckskei, A.; Mattaj, I. W. *Curr. Opin. Cell Biol.* **2005**, *17*, 27–34.
- (20) Ramos, J. L.; Duque, E.; Gallegos, M.-T.; Godoy, P.; Ramos-Gonzalez, M. I.; Rojas, A.; Teran, W.; Segura, A. *Annu. Rev. Microbiol.* **2002**, *56*, 743–768.
- (21) Mackay, D.; Shiu, W. Y. *J. Chem. Eng. Data* **1977**, *22*, 399–402.
- (22) Mackay, D.; Shiu, W. Y.; Ma, K. C. *Illustrated Handbook of Physical-chemical Properties and Environmental Fate for Organic Chemicals*; Lewis Publishers: Chelsea, MI, 1992; Vol. II.
- (23) Nelson, A. *Anal. Chim. Acta* **1987**, *194*, 139–149.
- (24) Qu, X.; Wang, X.; Zhu, D. *Environ. Sci. Technol.* **2007**, *41*, 8321–8327.
- (25) Contag, B. Z. *Naturforsch. C* **2005**, *60*, 799–806.
- (26) Castelli, F.; Librando, V.; Sarpietro, M. G. *Environ. Sci. Technol.* **2002**, *36*, 2717–2723.
- (27) Librando, V.; Sarpietro, M. G.; Castelli, F. *Environ. Toxicol. Pharmacol.* **2003**, *14*, 25–32.
- (28) Farkas, N.; Lorinczy, D.; Dergez, T.; Kilar, F.; Belagy, J. *Environ. Toxicol. Pharmacol.* **2004**, *16*, 163–168.
- (29) Bugg, T.; Foght, J. M.; Pickard, M. A.; Gray, M. R. *Appl. Environ. Microbiol.* **2000**, *66*, 5387–5392.
- (30) Miyata, N.; Iwahori, K.; Foght, J. M.; Gray, M. R. *Appl. Environ. Microbiol.* **2004**, *70*, 363–369.
- (31) Sikkema, J.; de Bont, J. A. M.; Poolman, B. *Microbiol. Rev.* **1995**, *59*, 201–222.
- (32) Whitman, B. E.; Lueking, D. R.; Mihelcic, J. R. *Can. J. Microbiol.* **1998**, *44*, 1086–1093.
- (33) Hearn, E. M.; Dennis, J. J.; Gray, M. R.; Foght, J. M. *J. Bacteriol.* **2003**, *185*, 6233–6240.
- (34) Tsitko, I. V.; Zaitsev, G. M.; Lobanok, A. G.; Salkinoja-Salonen, M. S. *Appl. Environ. Microbiol.* **1999**, *65*, 853–855.
- (35) Brown, G. R.; Sutcliffe, I. C.; Bendell, D.; Cummings, S. P. *FEMS Microbiol. Lett.* **2000**, *189*, 149–154.
- (36) Weber, F. J.; de Bont, J. A. M. *Biochim. Biophys. Acta* **1996**, *1286*, 225–245.
- (37) Heipieper, H. J.; Diefenbach, R.; Keweloh, H. *Appl. Environ. Microbiol.* **1992**, *58*, 1847–1852.
- (38) Unell, M.; Kabelitz, N.; Jansson, J. K.; Heipieper, H. J. *FEMS Microbiol. Lett.* **2007**, *266*, 138–143.
- (39) Gorria, M.; Tekpli, X.; Sergeant, O.; Huc, L.; Gaboriau, F.; Rissel, M.; Chevanne, M.; Dimanche-Boitrel, M.-T.; Lagadic-Gossmann, D. *Ann. N.Y. Acad. Sci.* **2006**, *1090*, 108–112.
- (40) Lommere, P. H. M.; Spaink, H. P.; Schmidt, T. *Biochim. Biophys. Acta* **2004**, *1664*, 119–131.
- (41) Munro, S. *Cell* **2003**, *115*, 377–388.
- (42) McConnell, H. M.; Vrljic, M. *Annu. Rev. Biophys. Biomol. Struct.* **2003**, *32*, 469–492.
- (43) Helms, J. B.; Zurzolo, C. *Traffic* **2004**, *5*, 247–254.
- (44) Parton, R. G.; Richards, A. A. *Traffic* **2003**, *4*, 724–738.
- (45) Zajchowski, L. D.; Robbins, S. M. *Eur. J. Biochem.* **2002**, *269*, 737–752.
- (46) Parton, R. G.; Hancock, J. F. *Trends Cell Biol.* **2004**, *14*, 141–147.
- (47) Brown, D. A.; London, E. *Annu. Rev. Cell Dev. Biol.* **1998**, *14*, 111–136.
- (48) Binder, W. H.; Barragan, V.; Menger, F. M. *Angew. Chem., Int. Ed. Engl.* **2003**, *42*, 5802–5827.
- (49) Edidin, M. *Annu. Rev. Biophys. Biomol. Struct.* **2003**, *32*, 257–283.
- (50) Ikonen, E. *Curr. Opin. Cell Biol.* **2001**, *13*, 470–477.
- (51) Mayor, S.; Rao, M. *Traffic* **2004**, *5*, 231–240.
- (52) Simons, K.; Ikonen, E. *Nature* **1997**, *387*, 569–572.
- (53) Thomas, J. L.; Holowka, D.; Baird, B.; Webb, W. W. *J. Cell Biol.* **1994**, *125*, 795–802.
- (54) Hao, M.; Mukherjee, S.; Maxfield, F. R. *Proc. Natl. Acad. Sci. U.S.A.* **2001**, *98*, 13072–13077.
- (55) Gidwani, A.; Holowka, D.; Baird, B. *Biochemistry* **2001**, *40*, 12422–12429.

- (56) Gaus, K.; Gratton, E.; Kable, E. P. W.; Jones, A. S.; Gelissen, I.; Kriparides, L.; Jessup, W. *Proc. Natl. Acad. Sci. U.S.A.* **2003**, *100*, 15554–15559.
- (57) Varma, R.; Mayor, S. *Nature* **1998**, *394*, 798–801.
- (58) Kusumi, A.; Ike, H.; Nakada, C.; Murase, K.; Fujiwara, T. *Semin. Immunol.* **2005**, *17*, 3–21.
- (59) Baumgart, T.; Hunt, G.; Farkas, E. R.; Webb, W. W.; Feigenson, G. W. *Biochim. Biophys. Acta* **2007**, *1768*, 2182–2194.
- (60) Corvis, Y.; Korchowiec, B.; Brezesinski, G.; Foliot, S.; Rogalska, E. *Langmuir* **2007**, *23*, 3338–3348.
- (61) Corvis, Y.; Barzyk, W.; Brezesinski, G.; Mrabet, N.; Badis, M.; Hecht, S.; Rogalska, E. *Langmuir* **2006**, *22*, 7701–7711.
- (62) Verger, R.; de Haas, G. H. *Chem. Phys. Lipids* **1973**, *10*, 127–136.
- (63) Aroti, A.; Leontidis, E.; Maltseva, E.; Brezesinski, G. *J. Phys. Chem. B* **2004**, *108*, 15238–15245.
- (64) Marra, J. J. *Colloid Interface Sci.* **1985**, *107*, 446–458.
- (65) Beitinger, H.; Vogel, V.; Moebius, D.; Rahmann, H. *Biochim. Biophys. Acta* **1989**, *984*, 293–300.
- (66) Hidalgo, A. A.; Caetano, W.; Tabak, M.; Oliveira, O. N. *Biophys. Chem.* **2004**, *109*, 85–104.
- (67) Korchowiec, B.; Paluch, M.; Corvis, Y.; Rogalska, E. *Chem. Phys. Lipids* **2006**, *144*, 127–136.
- (68) Corvis, Y.; Brezesinski, G.; Rink, R.; Walcarius, A.; Van der Heyden, A.; Mutelet, F.; Rogalska, E. *Anal. Chem.* **2006**, *78*, 1622–1630.
- (69) Cornut, I.; Desbat, B.; Turlet, J. M.; Dufourcq, J. *Biophys. J.* **1996**, *70*, 305–312.
- (70) Dziri, L.; Desbat, B.; Leblanc, R. M. *J. Am. Chem. Soc.* **1999**, *121*, 9618–9625.
- (71) Johann, R.; Vollhardt, D.; Mohwald, H. *Colloids Surf., A* **2001**, *182*, 311–320.
- (72) Blaudez, D.; Turlet, J.-M.; Dufourcq, J.; Bard, D.; Buffeteau, T.; Desbat, B. *J. Chem. Soc., Faraday Trans.* **1996**, *92*, 525–530.
- (73) Gelb, M. H.; Min, J.-H.; Jain, M. K. *Biochim. Biophys. Acta* **2000**, *1488*, 20–27.
- (74) Ferrato, F.; Carriere, F.; Sarda, L.; Verger, R. *Methods Enzymol.* **1997**, *286*, 327–347.
- (75) Warwicker, J. *FEBS Lett.* **1997**, *404*, 159–163.
- (76) Berg, O. G.; Gelb, M. H.; Tsai, M.-D.; Jain, M. K. *Chem. Rev.* **2001**, *101*, 2613–2653.
- (77) Scott, D. L.; Sigler, P. B. *Adv. Protein Chem.* **1994**, *45*, 53–88.
- (78) Carlson, P. A.; Gelb, M. H.; Yager, P. *Biophys. J.* **1997**, *73*, 230–238.
- (79) Rogalska, E.; Ransac, S.; Verger, R. *J. Biol. Chem.* **1993**, *268*, 792–794.
- (80) Rogalska, E.; Nury, S.; Douchet, I.; Verger, R. *Chirality* **1995**, *7*, 505–515.
- (81) Signor, G.; Mammi, S.; Peggion, E.; Ringsdorf, H.; Wagenknecht, A. *Biochemistry* **1994**, *33*, 6659–6670.
- (82) Grainger, D. W.; Reichert, A.; Ringsdorf, H.; Salesse, C.; Davies, D. E.; Lloyd, J. B. *Biochim. Biophys. Acta* **1990**, *1022*, 146–154.
- (83) Boroli, G. A.; Fanani, M. L.; Caputto, B. L.; Maggio, B. *Biochem. Biophys. Res. Commun.* **2002**, *295*, 964–969.
- (84) Fernandez, M. S.; Mejia, R.; Zavala, E. *Biochem. Cell Biol.* **1991**, *69*, 722–727.
- (85) Verheij, H. M.; Slotboom, A. J.; de Haas, G. H. *Rev. Physiol., Biochem. Pharmacol.* **1981**, *91*, 91–203.
- (86) Falahatpisheh, M. H.; Kerzee, J. K.; Metz, R. P.; Donnelly, K. C.; Ramos, K. S. *J. Carcinog.* **2004**, *3*, 1–8.
- (87) Edidin, M. *Nat. Rev., Mol. Cell Biol.* **2003**, *4*, 414–418.

JP804080H